Article

A Simple Flux-Side Formulation of State-Resolved Thermal Reaction Rates for Ring-Polymer Surface Hopping

Xuecheng Tao, Philip Shushkov, and Thomas Francis Miller

J. Phys. Chem. A, **Just Accepted Manuscript** • DOI: 10.1021/acs.jpca.9b00877 • Publication Date (Web): 22 Feb 2019

A Simple Flux-Side Formulation of State-Resolved Thermal Reaction Rates for Ring-Polymer Surface Hopping

Xuecheng Tao, Philip Shushkov, and Thomas F. Miller III*

Division of Chemistry and Chemical Engineering, California Institute of Technology, Pasadena, California 91125, USA

E-mail: *tfm@caltech.edu

Abstract

Employing the recently developed isomorphic Hamiltonian framework for including nuclear quantum effects in mixed quantum-classical non-adiabatic dynamics, we present a flux-side formulation of state-resolved thermal reaction rates for ring-polymer surface hopping (iso-RPSH). An appealing aspect of the new approach is that calculation of multiple state-resolved non-adiabatic thermal reaction rates is enabled with only a single free-energy surface calculation, whereas previous non-adiabatic flux-side formulations for surface hopping involve multiple free-energy surface calculations. The method is shown to be robust and straightforwardly implemented, and numerical results reveal that RPSH in the isomorphic Hamiltonian framework leads to better dividing-surface independence than alternative RPSH methods, due to improved preservation of the path-integral statistics.

Introduction

Ring polymer molecular dynamics (RPMD)[1–6] provides a simple method for including nuclear quantum effects (NQEs), such as zero-point energy and tunneling, in rate calculations for electronically adiabatic processes. RPMD is based on the imaginary time path-integral formalism[7–9] and captures NQEs by evolving classical trajectories of a ring-polymer Hamiltonian that exactly preserve quantum Boltzmann statistics. The RPMD thermal reaction rate is rigorously independent of the choice of dividing surface for the reaction,[3] numerically exact at high temperature limit and for a parabolic barrier,[2] and connected with instanton theory in the deep tunneling region.[10] These properties, in combination with favorable scaling of the computational cost of RPMD with respect to system size, have led it to be widely applied for the study of thermal reaction rates and mechanisms in complex systems.[11–25]

Recent effort has focused on extending RPMD for the description of processes involving multiple electronic states.[26–33] To this end, we recently introduced a multi-state isomorphic ring-polymer Hamiltonian[34] that allows for the inclusion of NQEs in any mixed quantum-classical (MQC) non-adiabatic dynamics method, including surface hopping,[35] Ehrenfest dynamics,[36] and other widely used methods.[37–41] The isomorphic Hamiltonian was shown to provide a natural and accurate way to combine RPMD with fewest switches surface hopping (i.e., iso-RPSH),[34] although the previously reported thermal rate calculations were performed using the relatively inefficient method of calculating rates from direct dynamics (i.e., without rare-event sampling). Here, we address this inefficiency by developing the theory for state-resolved iso-RPSH thermal re-

action rates in the flux-side formulation. The new approach has the appealing feature of requiring only a single free energy calculation to obtain the quantum transition state theory (QTST) rate, and the subsequent dynamical recrossing correction makes the rate prediction state-resolved and (nearly) dividing-surface independent. The method is illustrated in a model for the non-adiabatic F+H_2 reaction and compared to other implementations of ring-polymer surface hopping.

Method

We begin by reviewing the multi-state isomorphic ring-polymer Hamiltonian and its combination with fewest switches surface hopping.[34] The methodology is then extended for the calculation of state-resolved thermal rates in the flux-side formulation.

The isomorphic Hamiltonian

Consider a general Hamiltonian for a physical system with N electronic states in the diabatic representation,

$$\hat{H} = \frac{\hat{p}^2}{2m} + \mathbf{V}(\hat{q}), \tag{1}$$

where $\hat{p}$, $\hat{q}$ and m are the nuclear position, momentum, and mass, respectively. The physical potential, $\mathbf{V}$, is expressed as an $N \times N$ Hermitian matrix where the diagonal terms correspond to the diabatic potential energy surfaces and the off-diagonal terms correspond to electronic couplings. Throughout this paper, results are presented for a single nuclear degree of freedom, although extension to higher dimensions is straightforward.

By considering the path integral discretization of the canonical partition function, Q, we thus introduce the multi-state isomorphic ring-polymer Hamiltonian, $\mathbf{H}_n^{\mathrm{iso}}(\mathbf{p},\mathbf{q})$,[34] such that

$$\begin{aligned} Q &= \mathrm{tr}\left[e^{-\beta\hat{H}}\right] \\ &= \lim_{n\to\infty}\left(\frac{n}{2\pi\hbar}\right)^n \int d\mathbf{p}\, d\mathbf{q}\, \mathrm{tr_e}\left[e^{-\beta \mathbf{H}_n^{\mathrm{iso}}(\mathbf{p},\mathbf{q})}\right], \end{aligned} \tag{2}$$

where β and n are the inverse temperature and the number of imaginary time discretization steps, respectively. The vector $\mathbf{q} = \{q_1, q_2, \ldots, q_n\}$ represents the positions of the ring-polymer beads, and $\mathbf{p}$ represents the corresponding momenta. The symbol '$\mathrm{tr_e}$' denotes a partial trace over the electronic subspace. The resulting isomorphic Hamiltonian describes a ring-polymer comprised of n replicas, or beads, associated with copies of the original physical system,

$$\mathbf{H}_n^{\mathrm{iso}}(\mathbf{p},\mathbf{q}) = \sum_{\alpha=1}^{n} \frac{p_\alpha^2}{2m_n} + U_{\mathrm{spr}}(\mathbf{q}) + \mathbf{V}_n^{\mathrm{iso}}(\mathbf{q}) \tag{3}$$

with $m_n \equiv m/n$. Neighboring beads are connected by harmonic springs,

$$U_{\mathrm{spr}}(\mathbf{q}) = \frac{1}{2} m_n \omega_n^2 \sum_{\alpha=1}^{n} \left(q_\alpha - q_{\alpha+1}\right)^2, \tag{4}$$

where $\omega_n = (\beta_n \hbar)^{-1}$, $\beta_n = \beta/n$, and following Ref. 34, the isomorphic potential $\mathbf{V}_n^{\mathrm{iso}}$ is an $N \times N$ matrix that satisfies

$$\mu(\mathbf{q}) \equiv \mathrm{tr_e}\left[e^{-\beta \mathbf{V}_n^{\mathrm{iso}}(\mathbf{q})}\right] = \mathrm{tr_e}\left[\prod_{\alpha=1}^{n} e^{-\beta_n \mathbf{V}(q_\alpha)}\right] \tag{5}$$

and is chosen to have the form

$$\mathbf{V}_n^{\mathrm{iso}} = \mathbf{V}_n^{\mathrm{diag}} + \mathbf{V}_n^{\mathrm{coup}} + V_n^{\mathrm{mb}}\,\mathbb{I}, \tag{6}$$

where $\mathbb{I}$ is the identity matrix. The diagonal elements of the isomorphic potential correspond to the usual ring-polymer potentials associated with each diabatic state,

$$\left[\mathbf{V}_n^{\mathrm{diag}}(\mathbf{q})\right]_{ij} = \delta_{ij}\, \frac{1}{n} \sum_{\alpha=1}^{n} \left[\mathbf{V}(q_\alpha)\right]_{ii}. \tag{7}$$

with δ_{ij} the Kronecker delta function. The po-

tential coupling between pairs of states in the isomorphic potential is given by

$$[\mathbf{V}_n^{\mathrm{coup}}]_{ij}^2 = (1-\delta_{ij}) \times\Big\{\mathrm{acosh}^2\left[e^{\beta\left([\mathbf{V}_n^{\mathrm{diag}}]_{ii}+[\mathbf{V}_n^{\mathrm{diag}}]_{jj}\right)/2}\mu_{ij}/2\right]/\beta^2 - \left([\mathbf{V}_n^{\mathrm{diag}}]_{ii}-[\mathbf{V}_n^{\mathrm{diag}}]_{jj}\right)^2/4\Big\}, \tag{8}$$

where

$$\mu_{ij}(\mathbf{q}) = \mathrm{tr_e}\left[\prod_{\alpha=1}^{n}\exp\left(-\beta_n\begin{bmatrix}[\mathbf{V}(q_\alpha)]_{ii} & [\mathbf{V}(q_\alpha)]_{ij}\\ [\mathbf{V}(q_\alpha)]_{ji} & [\mathbf{V}(q_\alpha)]_{jj}\end{bmatrix}\right)\right], \tag{9}$$

and the sign of the potential coupling is kept to be the same as that of the physical potential evaluated at the ring-polymer centroid position. Lastly, the many-body potential term ensures that path-integral isomorphism (Eq. 2) is rigorously satisfied,

$$V_n^{\mathrm{mb}}(\mathbf{q}) = -\frac{1}{\beta}\ln\left\{\frac{\mu(\mathbf{q})}{\mathrm{tr_e}\left[e^{-\beta\left(\mathbf{V}_n^{\mathrm{diag}}(\mathbf{q})+\mathbf{V}_n^{\mathrm{coup}}(\mathbf{q})\right)}\right]}\right\}. \tag{10}$$

Like the standard ring-polymer Hamiltonian for a single-level system,[1] the Hamiltonian in Eq. 3 exploits the quantum-classical ring-polymer isomorphism, in the sense that Boltzmann sampling in the classical limit for the nuclear degrees of freedom on Eq. 3 yields the exact quantum Boltzmann distribution for the physical system.

iso-RPSH

An appealing feature of the isomorphic Hamiltonian (Eq. 3) is that it immediately can be combined with any mixed quantum-classical (MQC) dynamics method, thereby including nuclear quantum effects. The case for which the MQC method is trajectory surface hopping[35] leads to the iso-RPSH method.[34] For iso-RPSH, the evolution of the nuclei is described via the extended classical equations of motion

$$m_n\ddot{q}_\alpha = m_n\omega_n^2\left(q_{\alpha-1}+q_{\alpha+1}-2q_\alpha\right) - \frac{\partial}{\partial q_\alpha}\varepsilon_\gamma^{\mathrm{iso}}(\mathbf{q}), \tag{11}$$

where $\varepsilon_\gamma^{\mathrm{iso}}(\mathbf{q})$ is the γ^{th} adiabatic potential energy surface that is obtained by diagonalizing the isomorphic potential $\mathbf{V}_n^{\mathrm{iso}}(\mathbf{q})$, and the evolution of the electronic wavefunction, ψ, is described using the time-dependent Schrödinger equation along the nuclear trajectories,

$$i\hbar\frac{\partial}{\partial t}\psi(\mathbf{q},t) = \mathbf{V}_n^{\mathrm{iso}}(\mathbf{q})\psi(\mathbf{q},t). \tag{12}$$

As illustrated in Fig. 1, the ring-polymer evolves on a particular adiabatic potential energy surface until all ring-polymer beads simultaneously hop to a different adiabatic potential energy surface with probability

$$p_{\gamma\to\zeta} = \max\left\{-\frac{2}{a_{\gamma\gamma}}\mathrm{Re}\left(a_{\gamma\zeta}\sum_\alpha d_{\zeta\gamma}\dot{q}_\alpha\right)\Delta t,\ 0\right\}. \tag{13}$$

Here, $a_{\gamma\zeta}$ and $d_{\zeta\gamma}$ are the elements of the adiabatic electronic density matrix and first-derivative non-adiabatic coupling, respectively, and Δt is the propagation timestep. A hop can only occur under the condition of energy conservation, and hops are rejected if the ring polymer has insufficient velocity component along the non-adiabatic coupling vector; exactly as in classical surface hopping,[35] the velocity of each nuclear degree of freedom is modified along the direction of the non-adiabatic coupling vector. Although the current paper only presents results obtained using the Tully-surface hopping algorithm in its simplest form,[35] modified algorithms[42–44] including momentum reversal, decoherence corrections and extension to Liouvillian space can also be straightforwardly and unambiguously implemented in the isomorphic Hamiltonian framework.

Flux-side formulation of the iso-RPSH thermal rate

By extension of classical surface hopping rate theory,[45] the flux-side formulation of the RPSH

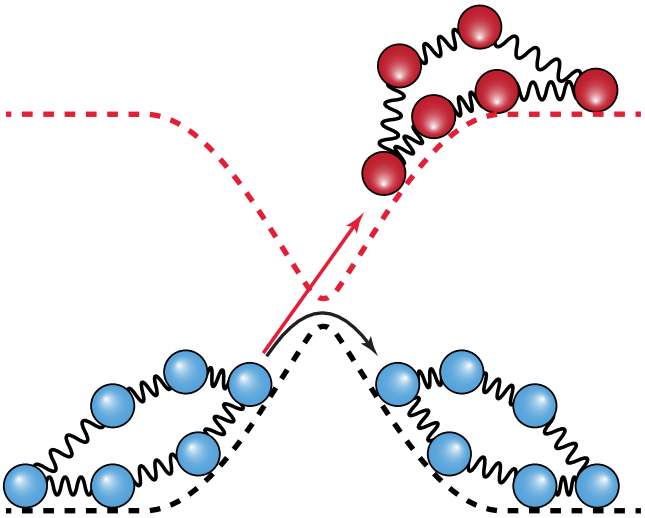

Figure 1: Schematic illustration of a hopping ring-polymer near avoided crossing. In RPSH dynamics, ring-polymer moves along a single surface until interrupted by instantaneous state transitions. The ring-polymers hop as a whole.

thermal reaction rate is[46]

$$k_{i\to f}^{\mathrm{RPSH}} Q_r = \lim_{n\to\infty}\lim_{t\to\infty}\left(\frac{n}{2\pi\hbar}\right)^n \int d\mathbf{p}_0 d\mathbf{q}_0\, \rho_n\left(\mathbf{p}_0,\mathbf{q}_0\right) \times \delta(\bar{q}_0 - q^{\ddagger})\,\bar{v}_0\, h(\bar{q}_t - q^{\ddagger})\,\delta_{i\theta_-t}\,\delta_{f\theta_t}. \quad (14)$$

Here, i and f specify the state upon which the system enter and exit, respectively, Q_r is the reactant partition function, and $t\to\infty$ defines a time period that is sufficiently long to allow for dynamical recrossing. The ring-polymer centroid position at time t is given by $\bar{q}_t$, and $\bar{v}_0$ denotes the initial centroid velocity, $\bar{v}_0 = \sum_\alpha \dot{q}_{0,\alpha}/n$. $q^{\ddagger}$ indicates the position of the dividing surface that separates the reactant and product regions in position space, and $\rho_n\left(\mathbf{p},\mathbf{q}\right)$ is the path-integral representation of the equilibrium quantum Boltzmann distribution for the multi-level system. The Heaviside function, $h(q-q^{\ddagger})$, is non-zero only if the position of the system is in the product region, and the Kronecker δ function, $\delta_{i\theta}$, is non-zero only if the system resides on adiabatic surface i, with θ_t specifying the active adiabatic surface upon which the RPSH trajectory resides at time t.

In the earlier work,[46] ρ_n was approximated using a Boltzmann-weighted sum of adiabatic ring-polymer surfaces,

$$\rho_n\left(\mathbf{p},\mathbf{q}\right) \simeq \sum_\gamma e^{-\beta H_{n,\gamma}(\mathbf{p},\mathbf{q})}, \quad (15)$$

where

$$H_{n,\gamma}(\mathbf{p},\mathbf{q}) = \sum_{\alpha=1}^{n}\frac{p_\alpha^2}{2m_n} + U_{\mathrm{spr}}(\mathbf{q}) + \frac{1}{n}\sum_{\alpha=1}^{n}\varepsilon_\gamma(q_\alpha), \quad (16)$$

and $\varepsilon_\gamma(q_\alpha)$ is the γ^{th} eigenvalue of the physical potential $\mathbf{V}(q_\alpha)$. A quantum transition state theory (QTST) rate[47,48] was computed for each adiabatic potential energy surface,

$$k_{\mathrm{QTST},\gamma}^{\mathrm{nokinks}}(q^{\ddagger}) Q_r = \lim_{n\to\infty}\left(\frac{n}{2\pi\hbar}\right)^n \int d\mathbf{p}_0 d\mathbf{q}_0\, e^{-\beta H_{n,\gamma}(\mathbf{p}_0,\mathbf{q}_0)} \times \delta(\bar{q}_0 - q^{\ddagger})\bar{v}_0\, h(\bar{p}_0), \quad (17)$$

to yield the state-resolved thermal rate,

$$k_{i\to f}^{\mathrm{nokinks-RPSH}} = \sum_\gamma k_{\mathrm{QTST},\gamma}^{\mathrm{nokinks}}(q^{\ddagger})\,\kappa_{i\to f,\gamma}(q^{\ddagger}), \quad (18)$$

where $\kappa_{i\to f,\gamma}$ is the recrossing factor[46] associated with trajectories that are initialized at the dividing surface on adiabat γ and that reside on adiabat i as $t\to-\infty$ and on adiabat f as $t\to\infty$. Here, the superscript "nokinks" is included to indicate the approximation to the path-integral statistics made in Eq. 15. Note that to calculate a single state-resolved rate, this protocol requires the independent calculation of N free energy surfaces and N recrossing factors.

In the current work, the quantum Boltzmann distribution is expressed exactly in terms of the isomorphic Hamiltonian,

$$\rho_n\left(\mathbf{p},\mathbf{q}\right) = \mathrm{tr_e}\left[e^{-\beta\mathbf{H}_n^{\mathrm{iso}}(\mathbf{p},\mathbf{q})}\right] \quad (19)$$

$$= e^{-\beta\mathbf{p}^{\mathrm{T}}\mathbf{p}/2m_n}\, e^{-\beta U_{\mathrm{spr}}(\mathbf{q})}\,\mu(\mathbf{q}) \quad (20)$$

$$= \sum_\gamma e^{-\beta H_{n,\gamma}^{\mathrm{iso}}(\mathbf{p},\mathbf{q})}, \quad (21)$$

where

$$H^{\rm iso}_{n,\gamma}(\mathbf{p},\mathbf{q}) = \sum_{\alpha=1}^{n} \frac{p_\alpha^2}{2m_n} + U_{\rm spr}(\mathbf{q}) + \varepsilon^{\rm iso}_\gamma(\mathbf{q}), \tag{22}$$

and $\varepsilon^{\rm iso}_\gamma(\mathbf{q})$ is the $\gamma^{\rm th}$ eigenvalue of the isomorphic potential, $\mathbf{V}^{\rm iso}_n(\mathbf{q})$. The analog of Eqs. 17 and 18 is still applicable with QTST rate now defined in terms of the adiabats of the isomorphic Hamiltonian, such that

$$k^{\rm iso}_{{\rm QTST},\gamma}(q^\ddagger)Q_r = \lim_{n\to\infty}\left(\frac{n}{2\pi\hbar}\right)^n \int d\mathbf{p}_0 d\mathbf{q}_0\, e^{-\beta H^{\rm iso}_{n,\gamma}(\mathbf{p}_0,\mathbf{q}_0)} \times \delta(\bar{q}_0 - q^\ddagger)\bar{v}_0\, h(\bar{p}_0). \tag{23}$$

The resulting expression for the state-resolved thermal rate is

$$k^{\rm iso-RPSH}_{i\to f} = \sum_\gamma k^{\rm iso}_{{\rm QTST},\gamma}(q^\ddagger)\,\kappa^{\rm iso}_{i\to f,\gamma}(q^\ddagger), \tag{24}$$

where the $\kappa^{\rm iso}_{i\to f,\gamma}(q^\ddagger)$ are the same state-resolved recrossing factors as in Eq. 18, except with trajectories run on the adiabats of the isomorphic Hamiltonian. As in Eq. 18, for a single state-resolved rate calculation, Eq. 24 requires the independent calculation of N free energy surfaces and N recrossing factors.

A central result of the current work is that by combining Eqs. 23 and 24 with Eq. 20, the state-resolved thermal rate expression can be formulated more simply,

$$k^{\rm iso-RPSH}_{i\to f} = k^{\rm MF}_{\rm QTST}(q^\ddagger)\,\kappa^{\rm iso}_{i\to f}(q^\ddagger), \tag{25}$$

in terms of a state-unresolved (i.e., mean-field) QTST,

$$k^{\rm MF}_{\rm QTST}(q^\ddagger)Q_r = \lim_{n\to\infty}\left(\frac{n}{2\pi\hbar}\right)^n \int d\mathbf{p}_0 d\mathbf{q}_0\, e^{-\beta H^{\rm MF}_n(\mathbf{p}_0,\mathbf{q}_0)} \times \delta(\bar{q}_0 - q^\ddagger)\bar{v}_0\, h(\bar{p}_0), \tag{26}$$

where

$$H^{\rm MF}_n(\mathbf{p},\mathbf{q}) = \sum_{\alpha=1}^{n} \frac{p_\alpha^2}{2m_n} + U_{\rm spr}(\mathbf{q}) - \frac{1}{\beta}\ln\mu(\mathbf{q}) \tag{27}$$

is the familiar mean-field (MF)-RPMD Hamiltonian.[26–28] In this formulation, state-resolution of the rate appears only via the dynamical recrossing factor,

$$\kappa^{\rm iso}_{i\to f}(q^\ddagger) = \frac{\lim_{n\to\infty}\lim_{t\to\infty}\int d\mathbf{p}_0 d\mathbf{q}_0\,\rho_n(\mathbf{p}_0,\mathbf{q}_0)\;\delta(\bar{q}_0 - q^\ddagger)\,\bar{v}_0\,h(\bar{q}_t - q^\ddagger)\,\delta_{i\theta_{-t}}\,\delta_{f,\theta_t}}{\lim_{n\to\infty}\int d\mathbf{p}_0 d\mathbf{q}_0\,\rho_n(\mathbf{p}_0,\mathbf{q}_0)\;\delta(\bar{q}_0 - q^\ddagger)\,\bar{v}_0\;h(\bar{p}_0)}. \tag{28}$$

Practical evaluation of the dynamical recrossing factor in Eq. 28 involves initialization of the iso-RPSH trajectories from the quantum Boltzmann distribution with the ring-polymer centroid constrained to the dividing surface. First, using that $\rho_n(\mathbf{p},\mathbf{q}) = e^{-\beta H^{\rm MF}_n(\mathbf{p},\mathbf{q})}$, nuclear configurations and velocities are sampled from the constrained distribution $e^{-\beta H^{\rm MF}_n(\mathbf{p}_0,\mathbf{q}_0)}\delta(\bar{q}_0 - q^\ddagger)$; then, using Eq. 21, the electronic state at the dividing surface, γ, is conditionally sampled from the Boltzmann weight of the isomorphic adiabatic surfaces at that ring-polymer nuclear configuration. The initialized trajectories are propagated both backwards and forwards in time using the iso-RPSH Hamiltonian in the adiabatic representation (Eq. 22) and with transitions induced by non-adiabatic couplings that are derived from Eq. 3. This leads to characterization of the position-space recrossing, as well as determination of the initial and final electronic state for each trajectory.

The primary advantage of the rate expres-

sion in Eq. 25 is that evaluation of the state-resolved reaction rates requires only the single MF-QTST in Eq. 26 and thus only a single free-energy calculation with respect to the well-behaved MF Hamiltonian in Eq. 27. This is a distinct feature of the method proposed here.

It is worth noting, however, that although the rate expression in Eq. 25 provides importance sampling with respect to the ring polymer nuclear configurations, it does not involve importance sampling with respect to the electronic states. That is, the electronic state of the trajectory at the dividing surface is sampled directly from the conditional probability distribution $\sum_\gamma e^{-\beta H^{\rm iso}_{n,\gamma}(\mathbf{p}_0,\mathbf{q}_0)}\delta(\bar{q}_0 - q^\ddagger)$, such that more trajectories will be initialized from electronic states that are thermally accessible at the dividing surface. As a result, the rate expression in Eq. 25 will provide a simple and efficient avenue to obtaining the state-resolved reaction rates that are most thermally accessible, whereas the rate expression in Eq. 24 may provide a more efficient means of obtaining state-resolved rates that make small contributions to the total thermal reaction rate.

Finally, we note that in direct analogy to Eqs. 25-27, the state-resolved thermal rate for the no-kinks approximation to RPSH can be expressed in terms of a state-unresolved MF-QTST, so that it too can be obtained with only a single free-energy calculation,

$$k_{i\to f}^{\rm nokinks-RPSH} = k_{\rm QTST}^{\rm MF-nokinks}(q^\ddagger)\,\kappa_{i\to f}^{\rm nokinks}(q^\ddagger), \tag{29}$$

in terms of a no-kinks approximation to the MF-QTST,

$$k_{\rm QTST}^{\rm MF-nokinks}(q^\ddagger)Q_r = \lim_{n\to\infty}\left(\frac{n}{2\pi\hbar}\right)^n \int d\mathbf{p}_0 d\mathbf{q}_0\, e^{-\beta H_n^{\rm MF-nokinks}(\mathbf{p}_0,\mathbf{q}_0)} \times \delta(\bar{q}_0 - q^\ddagger)\bar{v}_0\, h(\bar{p}_0), \tag{30}$$

where

$$H_n^{\rm MF-nokinks}(\mathbf{p},\mathbf{q}) = -\frac{1}{\beta}\ln\left(\sum_\gamma e^{-\beta H_{n,\gamma}(\mathbf{p},\mathbf{q})}\right). \tag{31}$$

Table 1: Parameter values for the potential of two-level reactive scattering model in Eq. 32.

Parameter	Value	Parameter	Value
A_1	7	a_1	1
A_2	$-18/\pi$	a_2	$\sqrt{3\pi}/4$
A_3	0.25	a_3	0.25
B_1	-0.75	q_1	-1.6
B_2	$54/\pi$	q_3	-2.625

For the evaluation of the recrossing factor in Eq. 29, the initialized trajectories are propagated both backwards and forwards in time using the nokinks-RPSH Hamiltonian in the adiabatic representation (Eq. 16)) and with transitions induced by non-adiabatic couplings that are averaged over the bead positions (i.e., the "bead approximation" from Ref. 46).

Computational Details

Calculations are presented for the one-dimensional, two-state model of gas-phase F+H_2 reactive scattering introduced in Ref. 34, which exhibits both substantial nuclear tunneling and electronically non-adiabatic effects.

Potential energy surfaces and couplings for the system in the diabatic representation are

$$\begin{aligned} V_1(q) &= \frac{A_1}{1+e^{-a_1(q-q_1)}} + B_1 \\ V_2(q) &= \frac{A_2}{1+e^{-a_2 q}} + \frac{B_2}{4\cosh^2(a_2 q/2)} \\ K_{12}(q) &= A_3 e^{-a_3(q-q_3)^2} \end{aligned} \tag{32}$$

with parameters given in Table 1. Both diabatic and adiabatic surfaces are plotted in Fig. 2A, with the reactant region at $q\to-\infty$ and the product region at $q\to\infty$. For the computed state-resolved thermal reaction rates, we will use the notation that k_1 indicates the rate for the system that entering on adiabat 1 and exiting to the product region on adiabat 1, and k_2 indicates the rate for the system that entering on adiabat 2 and exiting to the product region on adiabat 1. Note that the reaction channels are named here differently from those in Ref.

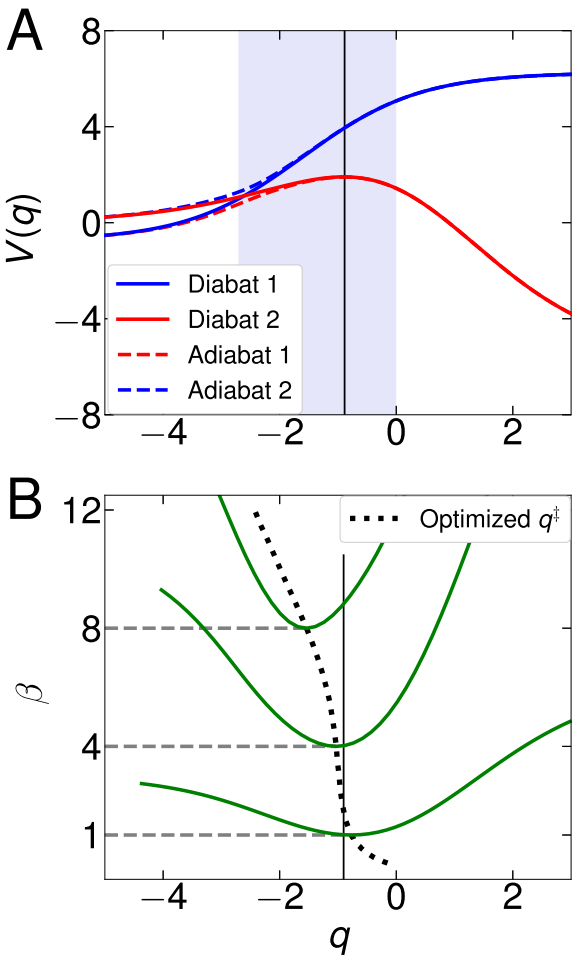

Figure 2: **(A)** Potential of the model system described as in Eq. 32. Diabatic and adiabatic states are shown in solid and dash lines, respectively. The filled area is the region in which following dividing surface independence tests are performed. **(B)** Optimized positions of the dividing surface as a function of reciprocal temperature is shown in the dotted line. Solid green lines depict the mean-field quantum transition state theory (MF-QTST, Eq. 26) rate on a log scale as a function of the dividing surface position for three different temperatures. Position of the reaction barrier on ground adiabat is indicated with a thin solid line.

34. We indicate the total (state-unresolved) thermal reaction rate as $k_{\rm total}$, mainly consisting of contributions from above two channels at the investigated temperature range $\beta \geq 1$. All the rate results below are reported in the unit of m·molecule^{-1} s^{-1}.

Three different surface hopping rate calculations are compared: (*i*) RPSH with the isomorphic Hamiltonian, called iso-RPSH, using Eqs. 25-27, (*ii*) RPSH with the no-kinks Hamiltonian, called nokinks-RPSH, using Eqs. 29-31, and (*iii*) classical surface hopping using the (shared) 1-bead limit of these expressions. We note that iso-RPSH employs an exact expression for the quantum Boltzmann distribution, nokinks-RPSH employs an approximate for the quantum Boltzmann distribution, and classical surface hopping employs the classical Boltzmann distribution. Exact quantum results are provided using wavepacket propagation the split-operator technique based.[49,50]

Each of the surface-hopping rate calculations is implemented in two stages - a statistical and a dynamical part. As in previous RPMD simulations,[12,13] the QTST rate for a biomolecular reaction is calculated using the Bennett-Chandler procedure.[51,52] An auxiliary dividing surface, q^*, is placed in the reactant asymptotic region, and the QTST rate is then given by

$$k_{\rm QTST}(q^\ddagger) = k_{\rm QTST}(q^*)\,\frac{k_{\rm QTST}(q^\ddagger)}{k_{\rm QTST}(q^*)} = \frac{1}{(2\pi\beta m)^{1/2}}\,\frac{\rho_c(q^\ddagger)}{\rho_c(q^*)} \qquad (33)$$

with

$$\rho_c(q^\ddagger) = \int d\mathbf{q}\, e^{-\beta U_{\rm spr}(\mathbf{q})}\,\mu(\mathbf{q})\,\delta(\bar{q} - q^\ddagger) \qquad (34)$$

the MF centroid density. For all the results presented in this section, QTST rates are obtained with importance sampling in the path-integral representation. Monte Carlo (MC) samplings with both 8β and 16β ring-polymer beads are conducted to make sure imaginary-time discretization convergence is reached. Statistical convergence is achieved for all the simulations with up to 10^9 MC moves. Optimized dividing surfaces in QTST calculations are obtained with a scan accurate to 0.01 a.u.

The dynamical recrossing factor κ is computed for each method by trajectory simulations. The ring-polymer Hamiltonian is integrated using the velocity Verlet algorithm,[53]

with the Liouville operator for nuclei motion factorized such that the free ring-polymer movements are solved analytically.[4,5] The isomorphic Hamiltonian and its derivatives are calculated using Bell's algorithm.[34] The electronic Schrödinger equation is evolved in the interaction representation with an unitary nuclear-position-coupled mid-point propagator[54] for four times during each nuclear timestep. The trajectories are initialized from a thermal distribution at the dividing surface. The thermal ensemble is generated using Metropolis algorithm while velocities are sampled from the Maxwell-Boltzmann distribution. Utilizing a standard reweighting strategy,[45] trajectories are first propagated backward in time to determine the correct quantum amplitude at the dividing surface, before they are propogated forward in time. The trajectories are simulated using a timestep of 0.0001 a.u. Dynamics simulation for ring-polymers with both 8β and 16β beads have been performed to check the convergence of the path-integral discretization. Rate results below are obtained using 10^5 trajectories, although we emphasize that to within graphical accuracy, identical results could have been obtained using only 10^3 trajectories. For the calculations reported with the dividing surface placed away from the optimized position, 8×10^5 trajectories are performed to fully describe the trajectory recrossing at each dividing surface position.

Results

We begin by demonstrating ring-polymer surface hopping (RPSH) in the flux-side formulation for a one-dimensional, two-state model of gas-phase F+H_2 reactive scattering (Fig. 2A). Given that the flux-side calculations involve a dynamical recrossing correction (Eq. 28, for example) to a QTST, Fig. 2B illustrates how the QTST estimate in Eq. 26 for the total thermal reaction rate varies as a function of the choice of dividing surface over a range of temperatures. Consistent with previous observations of electronically adiabatic RPMD,[3] the optimal position of the dividing surface shifts away from the position of the barrier-top for the ground-state adiabat at lower temperatures ($\beta > 1$), due to significant nuclear tunneling effects. However, in a strictly non-adiabatic effect, Fig. 2B also shows that the optimal position of the dividing surface shifts away from the barrier-top position at high temperatures ($\beta < 1$), due to the influence of the excited electronic state.

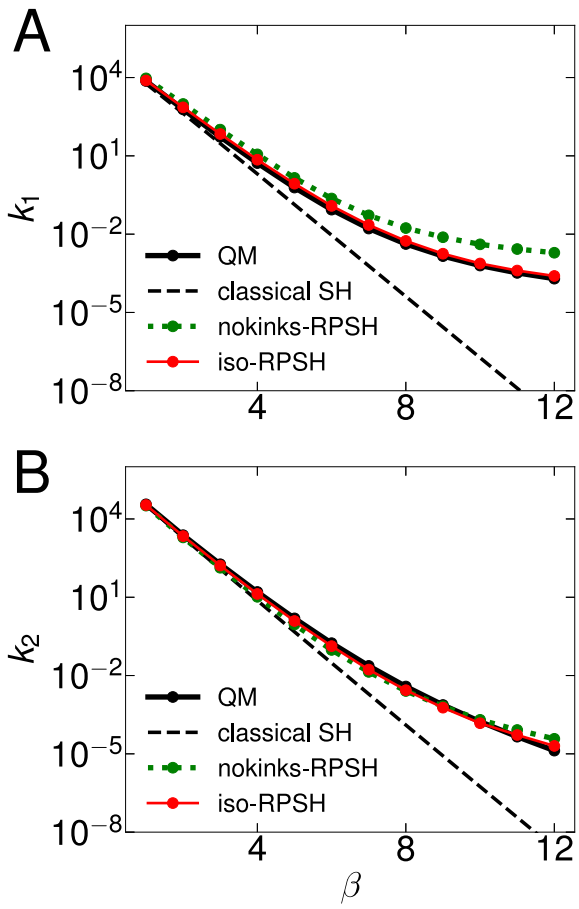

Figure 3: Arrhenius plots of state-resolved thermal rates versus reciprocal temperature for two reaction channels, **(A)** adiabat $1 \rightarrow 1$ and **(B)** adiabat $2 \rightarrow 1$. Rates are calculated from exact quantum mechanics (QM, thick solid black), classical surface hopping (classical SH, dashed black), ring-polymer surface hopping dynamics with the no-kinks approximation (nokinks-RPSH, dotted green) and RPSH in the isomorphic Hamiltonian framework (iso-RPSH, solid red). Mean standard deviations for all the data points plotted are smaller than the size of markers. Dividing surfaces in the RPSH calculations are placed at the optimal positions.

Fig. 3 presents the state-resolved thermal reaction rate versus inverse temperature for two different reactive channels, obtained using exact quantum mechanics, classical surface hopping, iso-RPSH,[34] and nokinks-RPSH.[46] As is clear from comparison of the exact quantum results and classical surface hopping, the nuclear tunneling effects accelerate the reaction rate and becomes more significant at lower temperatures. Flux-side formulation of iso-RPSH dynamics provides accurate state-resolved rates for the full range of temperatures, as seen previously when employed with the side-side formulation of the rate.[34] The key difference using the flux-side formulation in the current work is that substantially smaller statistical errors are achieved with 1000-fold fewer dynamical trajectories than in the previous study. The nokinks-RPSH method overestimates the rate for both channel, but the effect is much more stubstantial for rate k_1, which corresponds to the system entering and exiting on the lower electronic adiabat; the deviation of nokinks-RPSH from exact results is due to underestimation of the influence of the low-lying excited state, which acts to suppress the rate (see for example, Fig. 2 in Ref. 21).

We now explore the robustness of the RPSH methods to the choice of dividing surface position. The RPSH calculations in Fig. 3 were obtained using the flux-side formulation with the optimal choice of dividing surface for the associated MF-QTST (i.e., Eq. 26 for iso-RPSH and Eq. 30 for the nokinks-RPSH). For the inverse temperature $\beta = 8$, Fig. 4A presents total (state-unresolved) thermal reaction rate for the reaction, using a variety of methods, as a function of the dividing surface position. As is necessary,[55] the exact quantum mechanical rate is strictly independent of the choice of dividing surface, and in stark contrast, the MF-QTST of Eq. 26 is exponentially dependent on the position of the dividing surface. The classical surface hopping result differ substantially from the quantum result due to the exclusion of nuclear tunneling effects, and as has been seen previously,[56] they vary as a function of dividing surface position due to inexact preservation of the mixed quantum-classical Boltzmann distribution by the dynamical trajectories,[57,58] although the degree of variation (∼40%) is small

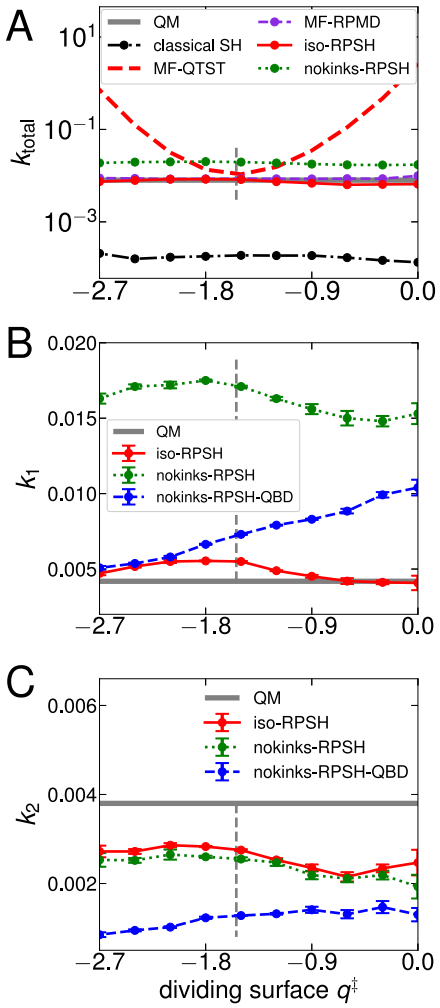

Figure 4: Dividing surface dependence of thermal rates at $\beta = 8$ for **(A)** state-unresolved total rate, channels **(B)** adiabat $1 \to 1$, and **(C)** adiabat $2 \to 1$. Rates are calculated from exact quantum mechanics (QM, thick grey), classical surface hopping (classical SH, dash-dotted black), mean-field quantum transition state theory (MF-QTST, dashed red, Eq. 26), mean-field ring polymer molecular dynamics (MF-RPMD, dashed violet), and three implementations of ring-polymer surface hopping as described in the main text (RPSH, solid red, dashed blue and dotted green lines). For data points error bars are not explicitly shown, mean standard deviations are smaller than the size of markers. Optimal positions for the dividing surface are shown in dashed grey.

on the scale of this plot. Both RPSH methods likewise vary slightly on this scale as a function of dividing surface position due to inexact preservation of the quantum Boltzmann distribution by the dynamical trajectories. Notably, the rate obtained using MF-RPMD is strictly independent of the dividing surface position due to exact preservation of the quantum Boltzmann distribution by the dynamical trajectories, although this method has the disadvantage of not enabling state-resolved rate calculations.

Figs. 4B and C present the state-resolved thermal reaction rate for the adiabat $1 \rightarrow 1$ channel (k_1) and the adiabat $2 \rightarrow 1$ channel (k_2), computed using exact quantum mechanics, iso-RPSH (red), and nokinks-RPSH (green). Again, it is seen that the exact quantum results are strictly independent of the position of the dividing surface, and as in Fig. 3, it is seen that nokinks-RPSH (green) substantially overestimates the k_1 rate while iso-RPSH (red) provides the best estimate of both channels. Given the more narrow range of rates plotted in these panels, the variation of the RPSH methods is more clearly seen with both iso-RPSH and nokinks-RPSH varying by a similar degree ($\sim$25%) as a function of dividing surface position.

Also shown in Figs. 4B and C is the result of a rate expression that uses MF-QTST with the exact quantum Boltzmann distribution (Eq. 26), while the recrossing factor is evaluated by trajectories that are initialized from the exact quantum Boltzmann distribution and are propagated using nokinks-RPSH dynamics. Whereas this hybrid method, analogs of which have been suggested in other contexts,[27] improves the rate associated with the lower adiabat (k_1), it does so at the cost of introducing a much stronger dependence on the position of the dividing surface. This example illustrates the statistical importance of kinked ring-polymer configurations in describing these non-adiabatic reaction rates, as well as the fact that iso-RPSH does a substantially better job of preserving the true quantum Boltzmann distribution than the nokinks-RPSH method.

Summary

The development of practical, robust, and accurate quantum methods that incorporate both nuclear quantum effects and allow for electronically non-adiabatic transitions remains an important challenge for the description of complex photochemical, charge-transfer, and energy-transfer processes. In this work, we present an efficient flux-side formulation of ring-polymer surface hopping on the isomorphic path-integral Hamiltonian (iso-RPSH). The method is straightforwardly implemented, involving no greater complexity than a standard trajectory surface hopping rate calculation, and it is shown to be accurate and relatively insensitive to the position of the transition-state dividing surface. A novel and appealing aspect of the flux-side formulation presented here is that calculation of multiple state-resolved non-adiabatic thermal reaction rates is enabled with only a single free-energy surface calculation. The combined accuracy and simplicity of iso-RPSH make it amenable to useful application in realistic chemical systems.

Acknowledgement We acknowledge support from the Office of Naval Research under Award Number N00014-10-1-0884. Additionally, P.S. acknowledges a German Research Foundation (DFG) Postdoctoral Fellowship. Computational resources were provided by the National Energy Research Scientific Computing Center, which is supported by the Office of Science of the US Department of Energy under Contract No. DE-AC02-05CH11231.

References

(1) Craig, I. R.; Manolopoulos, D. E. Quantum Statistics and Classical Mechanics: Real Time Correlation Functions From Ring Polymer Molecular Dynamics. *J. Chem. Phys.* **2004**, *121*, 3368–3373.

(2) Craig, I. R.; Manolopoulos, D. E. Chemical Reaction Rates From Ring Poly-

mer Molecular Dynamics. *J. Chem. Phys.* **2005**, *122*, 084106.

(3) Craig, I. R.; Manolopoulos, D. E. A Refined Ring Polymer Molecular Dynamics Theory Of Chemical Reaction Rates. *J. Chem. Phys.* **2005**, *123*, 034102.

(4) Miller III, T. F.; Manolopoulos, D. E. Quantum Diffusion In Liquid Para-Hydrogen From Ring-Polymer Molecular Dynamics. *J. Chem. Phys.* **2005**, *122*, 184503.

(5) Miller III, T. F.; Manolopoulos, D. E. Quantum Diffusion In Liquid Water From Ring Polymer Molecular Dynamics. *J. Chem. Phys.* **2005**, *123*, 154504.

(6) Habershon, S.; Manolopoulos, D. E.; Markland, T. E.; Miller III, T. F. Ring-Polymer Molecular Dynamics: Quantum Effects In Chemical Dynamics From Classical Trajectories In an Extended Phase Space. *Annu. Rev. Phys. Chem.* **2013**, *64*, 387–413.

(7) Feynman, R. P.; Hibbs, A. R. *Quantum Mechanics and Path Integrals*; McGraw-Hill, 1965.

(8) Chandler, D.; Wolynes, P. G. Exploiting the Isomorphism Between Quantum Theory and Classical Statistical Mechanics Of Polyatomic Fluids. *J. Chem. Phys.* **1981**, *74*, 4078–4095.

(9) Parrinello, M.; Rahman, A. Study Of an F Center In Molten Kcl. *J. Chem. Phys.* **1984**, *80*, 860–867.

(10) Richardson, J. O.; Althorpe, S. C. Ring-Polymer Molecular Dynamics Rate-Theory In the Deep-Tunneling Regime: Connection With Semiclassical Instanton Theory. *J. Chem. Phys.* **2009**, *131*, 214106.

(11) Suleimanov, Y. V.; Aoiz, F. J.; Guo, H. Chemical Reaction Rate Coefficients From Ring Polymer Molecular Dynamics: Theory and Practical Applications. *J. Phys. Chem. A* **2016**, *120*, 8488–8502.

(12) Collepardo-Guevara, R.; Suleimanov, Y. V.; Manolopoulos, D. E. Bimolecular Reaction Rates From Ring Polymer Molecular Dynamics. *J. Chem. Phys.* **2009**, *130*, 174713.

(13) Suleimanov, Y. V.; Collepardo-Guevara, R.; Manolopoulos, D. E. Bimolecular Reaction Rates From Ring Polymer Molecular Dynamics: Application To H+ CH_4 → H_2+ CH_3. *J. Chem. Phys.* **2011**, *134*, 044131.

(14) Perez de Tudela, R.; Aoiz, F.; Suleimanov, Y. V.; Manolopoulos, D. E. Chemical Reaction Rates From Ring Polymer Molecular Dynamics: Zero Point Energy Conservation In Mu+ H_2 → MuH+ H. *J. Phys. Chem. Lett.* **2012**, *3*, 493–497.

(15) Suleimanov, Y. V.; de Tudela, R. P.; Jambrina, P. G.; Castillo, J. F.; Sáez-Rábanos, V.; Manolopoulos, D. E.; Aoiz, F. J. A Ring Polymer Molecular Dynamics Study Of the Isotopologues Of the H+ H_2 Reaction. *Phys. Chem. Chem. Phys.* **2013**, *15*, 3655–3665.

(16) Li, Y.; Suleimanov, Y. V.; Yang, M.; Green, W. H.; Guo, H. Ring Polymer Molecular Dynamics Calculations Of Thermal Rate Constants For the O (3P)+ CH_4 → OH + CH_3 Reaction: Contributions Of Quantum Effects. *J. Phys. Chem. Lett.* **2012**, *4*, 48–52.

(17) Li, Y.; Suleimanov, Y. V.; Li, J.; Green, W. H.; Guo, H. Rate Coefficients and Kinetic Isotope Effects Of the X+ CH_4 → CH_3+ HX (X= H, D, Mu) Reactions From Ring Polymer Molecular Dynamics. *J. Chem. Phys.* **2013**, *138*, 094307.

(18) Suleimanov, Y. V. Surface Diffusion Of Hydrogen On Ni (100) From Ring Polymer Molecular Dynamics. *J. Phys. Chem. C* **2012**, *116*, 11141–11153.

(19) Boekelheide, N.; Salomón-Ferrer, R.; Miller III, T. F. Dynamics and Dissipation

In Enzyme Catalysis. *Proc. Natl. Acad. Sci. U.S.A.* **2011**, *108*, 16159–16163.

(20) Kretchmer, J. S.; Boekelheide, N.; Warren, J. J.; Winkler, J. R.; Gray, H. B.; Miller, T. F. Fluctuating Hydrogen-Bond Networks Govern Anomalous Electron Transfer Kinetics In a Blue Copper Protein. *Proc. Natl. Acad. Sci. U.S.A.* **2018**, *115*, 6129–6134.

(21) Kretchmer, J. S.; Miller III, T. F. Direct Simulation Of Proton-Coupled Electron Transfer Across Multiple Regimes. *J. Chem. Phys.* **2013**, *138*, 04B602.

(22) Kretchmer, J. S.; Miller III, T. F. Tipping the Balance Between Concerted Versus Sequential Proton-Coupled Electron Transfer. *Inorg. Chem.* **2015**, *55*, 1022–1031.

(23) Castillo, J.; Suleimanov, Y. A Ring Polymer Molecular Dynamics Study Of the OH+ H2 (D2) Reaction. *Phys. Chem. Chem. Phys.* **2017**, *19*, 29170–29176.

(24) Miller III, T. F. Isomorphic Classical Molecular Dynamics Model For an Excess Electron In a Supercritical Fluid. *J. Chem. Phys.* **2008**, *129*, 194502.

(25) Menzeleev, A. R.; Miller III, T. F. Ring Polymer Molecular Dynamics Beyond the Linear Response Regime: Excess Electron Injection and Trapping In Liquids. *J. Chem. Phys.* **2010**, *132*, 034106.

(26) Hele, T. J. Master's Thesis, Exeter College, Oxford University, 2011.

(27) Duke, J. R.; Ananth, N. Mean Field Ring Polymer Molecular Dynamics For Electronically Nonadiabatic Reaction Rates. *Faraday Discuss.* **2017**, *195*, 253–268.

(28) Menzeleev, A. R.; Bell, F.; Miller III, T. F. Kinetically Constrained Ring-Polymer Molecular Dynamics For Non-Adiabatic Chemical Reactions. *J. Chem. Phys.* **2014**, *140*, 064103.

(29) Kretchmer, J. S.; Miller III, T. F. Kinetically-Constrained Ring-Polymer Molecular Dynamics For Non-Adiabatic Chemistries Involving Solvent and Donor–Acceptor Dynamical Effects. *Faraday Discuss.* **2016**, *195*, 191–214.

(30) Ananth, N. Mapping Variable Ring Polymer Molecular Dynamics: a Path-Integral Based Method For Nonadiabatic Processes. *J. Chem. Phys.* **2013**, *139*, 124102.

(31) Pierre, S.; Duke, J. R.; Hele, T. J.; Ananth, N. A Mapping Variable Ring Polymer Molecular Dynamics Study Of Condensed Phase Proton-Coupled Electron Transfer. *J. Chem. Phys.* **2017**, *147*, 234103.

(32) Richardson, J. O.; Thoss, M. Communication: Nonadiabatic Ring-Polymer Molecular Dynamics. *J. Chem. Phys.* **2013**, *139*, 031102.

(33) Chowdhury, S. N.; Huo, P. Coherent State Mapping Ring Polymer Molecular Dynamics For Non-Adiabatic Quantum Propagations. *J. Chem. Phys.* **2017**, *147*, 214109.

(34) Tao, X.; Shushkov, P.; Miller III, T. F. Path-Integral Isomorphic Hamiltonian For Including Nuclear Quantum Effects In Non-Adiabatic Dynamics. *J. Chem. Phys.* **2018**, *148*, 102327.

(35) Tully, J. C. Molecular Dynamics With Electronic Transitions. *J. Chem. Phys.* **1990**, *93*, 1061–1071.

(36) Ehrenfest, P. Bemerkung Über Die Angenäherte Gültigkeit Der Klassischen Mechanik Innerhalb Der Quantenmechanik. *Zeitschrift für Physik a Hadrons and Nuclei* **1927**, *45*, 455–457.

(37) Kapral, R.; Ciccotti, G. Mixed Quantum-Classical Dynamics. *J. Chem. Phys.* **1999**, *110*, 8919–8929.

(38) Nielsen, S.; Kapral, R.; Ciccotti, G. Statistical Mechanics Of Quantum-Classical

Systems. *J. Chem. Phys.* **2001**, *115*, 5805–5815.

(39) Nielsen, S.; Kapral, R.; Ciccotti, G. Mixed Quantum-Classical Surface Hopping Dynamics. *J. Chem. Phys.* **2000**, *112*, 6543–6553.

(40) Miller, W. H.; Cotton, S. J. Classical Molecular Dynamics Simulation Of Electronically Non-Adiabatic Processes. *Faraday Discuss.* **2016**, *195*, 9–30.

(41) Cotton, S. J.; Miller, W. H. Symmetrical Windowing For Quantum States In Quasi-Classical Trajectory Simulations. *J. Phys. Chem. A* **2013**, *117*, 7190–7194.

(42) Hammes-Schiffer, S.; Tully, J. C. Proton Transfer In Solution: Molecular Dynamics With Quantum Transitions. *J. Chem. Phys.* **1994**, *101*, 4657–4667.

(43) Subotnik, J. E.; Shenvi, N. A New Approach To Decoherence and Momentum Rescaling In the Surface Hopping Algorithm. *J. Chem. Phys.* **2011**, *134*, 024105.

(44) Wang, L.; Sifain, a. E.; Prezhdo, O. V. Fewest Switches Surface Hopping In Liouville Space. *J. Phys. Chem. Lett.* **2015**, *6*, 3827–3833.

(45) Hammes-Schiffer, S.; Tully, J. C. Nonadiabatic Transition State Theory and Multiple Potential Energy Surface Molecular Dynamics Of Infrequent Events. *J. Chem. Phys.* **1995**, *103*, 8528–8537.

(46) Shushkov, P.; Li, R.; Tully, J. C. Ring Polymer Molecular Dynamics With Surface Hopping. *J. Chem. Phys.* **2012**, *137*, 22A549.

(47) Voth, G. a.; Chandler, D.; Miller, W. H. Rigorous Formulation Of Quantum Transition State Theory and Its Dynamical Corrections. *J. Chem. Phys.* **1989**, *91*, 7749–7760.

(48) Hele, T. J.; Althorpe, S. C. Derivation Of a True ($t \rightarrow 0+$) Quantum Transition-State Theory. I. Uniqueness and Equivalence To Ring-Polymer Molecular Dynamics Transition-State-Theory. *J. Chem. Phys.* **2013**, *138*, 084108.

(49) Feit, M.; Fleck Jr, J.; Steiger, a. Solution Of the Schrödinger Equation By a Spectral Method. *J. Comput. Phys.* **1982**, *47*, 412–433.

(50) Neuhauser, D.; Baer, M.; Judson, R. S.; Kouri, D. J. The Application Of Time-Dependent Wavepacket Methods To Reactive Scattering. *Comput. Phys. Commun.* **1991**, *63*, 460–481.

(51) Bennett, C. H. *Algorithms For Chemical Computations*; American Chemical Society, 1977.

(52) Chandler, D. Statistical Mechanics Of Isomerization Dynamics In Liquids and the Transition State Approximation. *J. Chem. Phys.* **1978**, *68*, 2959–2970.

(53) Frenkel, D.; Smit, B. *Understanding Molecular Simulation: From Algorithms To Applications*; Academic press, 2001.

(54) Li, X.; Tully, J. C.; Schlegel, H. B.; Frisch, M. J. Ab Initio Ehrenfest Dynamics. *J. Chem. Phys.* **2005**, *123*, 084106.

(55) Miller, W. H.; Schwartz, S. D.; Tromp, J. W. Quantum Mechanical Rate Constants For Bimolecular Reactions. *J. Chem. Phys.* **1983**, *79*, 4889–4898.

(56) Jain, A.; Subotnik, J. E. Surface Hopping, Transition State Theory, and Decoherence. II. Thermal Rate Constants and Detailed Balance. *J. Chem. Phys.* **2015**, *143*, 134107.

(57) Parandekar, P. V.; Tully, J. C. Mixed Quantum-Classical Equilibrium. *J. Chem. Phys.* **2005**, *122*, 094102.

(58) Schmidt, J.; Parandekar, P. V.; Tully, J. C. Mixed Quantum-Classical

Equilibrium: Surface Hopping. *J. Chem. Phys.* **2008**, *129*, 044104.

Graphical TOC Entry